Signatures of Discrete Breathers in Coherent State Quantum Dynamics

Kirill Igumenshchev,^{1,*} Misha Ovchinnikov,^{1,†} Panagiotis Maniadis,^{2,‡} and Oleg Prezhdo^{1,§}

¹Department of Chemistry, University of Rochester, Rochester, NY 14627

²Theoretical Division, Los Alamos National Laboratory, Los Alamos, NM 87545

(Dated: November 27, 2024)

Abstract

Discrete breathers (DBs) – a spatial time-periodic localization of energy – are predicted in a

large variety of non-linear systems. Motivated by the conceptual bridging of the DBs phenomena

in classical and quantum mechanical representation, we study their signatures in the dynamics

of a quantum equivalent of a classical mechanical point in a phase space – a coherent state. We

show that in contrast to a point in a phase space that can exhibit either delocalized or localized

motion, a coherent state can show signatures of a quantum equivalent of both localized and de-

localized behavior. In classical mechanics, the separation between the energy regions of localized

and delocalized motion is a point. In quantum mechanics, this point becomes a transient region,

in which both tunneling and non-tunneling modes are present. Furthermore, the transient region

contains modes that cannot be characterized as either, because the transition from non-tunneling

to tunneling modes is smooth. With a further analysis we document four intriguing observations:

1. Considered as a function of coupling, the eigenstates go through avoided crossings between

tunneling and non-tunneling modes. 2. The dominance of tunneling modes in high non-linearity

region is compromised by an appearance of new types of modes – high order tunneling modes.

These modes are similar to the tunneling modes but have attributes of non-tunneling modes. 3.

There are types of excitations, which prioritize higher order tunneling modes and allows us to study

their properties. 4. For high non-linearity, the auto-correlation function decreases fast; therefore,

short-times dynamics is sufficient for modeling quantum DBs. This work provides a foundation

for implementation of modern semi-classical methods to model quantum DBs, bridging concepts of

classical and quantum mechanical signatures of DBs, and understanding spectroscopic experiments

that involve a coherent state.

PACS numbers: 03.65.Ge, 63.20.Pw, 03.65.Sq, 03.65.Xp

Keywords:

*kigumens@mail.rochester.edu

†ovchinnikov@chem.rochester.edu

[‡]maniadis@lanl.gov

§oleg.prezhdo@rochester.edu

2

I. INTRODUCTION

Understanding the mechanism of quantum discrete breathers (QDBs) is important for a number of application areas, including medicine [1], nano-materials [2–4] and quantum computers [5]. From the classical mechanics perspective, discrete breathers (DBs) is a fairly well understood phenomena, and occur when energy localizes in the system for an infinite amount of time. The effect is due to an interplay of non-linearity of the sites' potentials and coupling between the sites. In quantum mechanical perspective, the phenomena is different; a localization in quantum symmetric potential is not possible due to tunneling. Experimentally, one can observe traces of QDBs breathers in the form of anomaly long localization time [?]. QDBs have been observed in crystals [3, 4, 6], Bose-Einstein condensates [7] and interacting Josephson junctions [5]. Complimenting the experiments, theoretical solutions of QDBs stems from quantizing classical solutions for both integrable [8] and non-integrable systems [9]. Theoretically, DBs have been studied in a number of systems of a practical importance: molecules [10], biological polymers [1], quantum dots [2], nano-tubes [11] and graphene sheets [12].

Investigating the quantum dynamics of a coherent state targets two areas of research: bridging classical and quantum description of DBs and building a foundation for numerical methods that use coherent states. A coherent state is a quantum equivalent of a point in a classical phase space. Comparing signatures of DBs in dynamics of a point in a classical phase space and a coherent states, outlines the conceptual differences and similarities between classical and quantum descriptions of DBs. Even numerically, large experimentally accessible systems are difficult to model using exact quantum dynamics methods. One needs approximations that keep track of quantum effects and scale well with system size. A number of methods that rely on time-evolution of a coherent state, such as QHD [13], Herman-Kluk (HK) propagator [14] and its higher order extensions [15, 16], coupled coherent states (CCS) [17], matching-pursuit/split-operator Fourier transform (MP-SOFT) [18, 19] and coherentstate path-integral (CSPI) [20], are effective for large systems. These methods have been successfully used only for slightly non-linear systems; in addition, these methods were derived to be applied to harmonic or slightly anharmonic system. Modeling highly non-linear phenomena such as DBs can be a challenge. With an exception of QHD [21], these methods have not been applied to QDBs. Studying the quantum dynamics of a coherent state will show the limitations of these techniques when applied to QDBs.

The current study is related to previous work on modeling DBs in systems that may have quantum effects, fundamental theory on QDBs, and the applicability of semi-classical methods. Due to the high computational cost of quantum simulation, systems of practical importance that contain quantum effects [1, 2, 10–12] are simulated with classical dynamics. Our work illustrates limitations of classical dynamics by outlining quantum effects in the dynamics of a coherent state. Previous theoretical work on QDBs manifests from the quantization of an integrable [8] and non-integrable [9] dimer, the analysis of a splitting of QDBs modes [22] and existence of an avoided crossing [23]. We build on this work by providing an analysis of coherent states rather than eigenstates. Conventionally QDBs are studied by finding eigenstates of the system's Hamiltonian [24]. Since here we are interested in the dynamics of a coherent state rather than eigenstates, our approach involves simulating the dynamics of a superposition of eigenstates in a form of a coherent state. Motivation for this project came from our work on applying QHD [21] and HK [25] semi-classical methods to model QDBs; in these two works, the influence of tunneling modes (a quantum mechanical equivalent of DB modes) on the quantum dynamics of coherent state was unresolved.

Here, we focus on the fundamental concepts of QDBs in coherent state dynamics that build foundation to practical applications. Our approach is to study the dynamics of a coherent state in the simplest quantum mechanical Hamiltonian that accounts for QDBs phenomena. We choose a two-site quartic potential with a linear coupling. To study the transfer and localization of energy, we start by displacing a coherent state on one of the sites, while keeping the other site in a ground state. Analysis of the spectrum will provide insight into the behavior of the coherent state. Contour plots of the distribution of the eigenstate wave-function between the sites will give a more detailed analysis of energy between the sites for a specific eigenstate. Spectrum and contour plots help us to draw conclusions regarding the earlier mentioned problems.

The paper is structured in following way: In the following section we discuss methods and numerical procedures. The results section starts with an analysis of the dynamics of the coherent state by investigating the spectrum. The second part of the results shows a transient region, a region with both tunneling and non-tunneling modes. The last part of the results briefly discusses existence of the following effects: avoided crossing between tunneling and non-tunneling modes, manifestation of higher order tunneling modes (HOTM), control

of HOTM intensity with initial displacement, and rapid decrease of autocorrelation function due to non-linearity. The last section will outline our findings and their importance.

II. SYSTEM AND METHODS

Breathers appear in a wide range of systems. We consider a simple model system that is computationally accessible, conceptually simple and congruent with natural systems: a Hamiltonian with quartic oscillators and linear coupling:

$$H = c_h(P_1^2 + P_2^2 + X_1^2 + X_2^2) + c_a(X_1^4 + X_2^4) + c_cX_1X_2$$
(1)

Here, P_1 , P_2 , X_1 and X_2 are either classical coordinates or quantum mechanical operators, c_h is a harmonic constant with the value " $\frac{1}{2}$ ", c_a is responsible for the anharmonicity of the potential, and c_c is a linear coupling coefficient.

The phenomena of DBs and QDBs are due to non-linearities in the potential. When the oscillators are in low energy states, the quadratic term dominates over the quartic term – the motion is harmonic. There is an exchange of energy between the oscillators. However, suppose one of the oscillators is higher in energy. The quartic term dominates over the quadratic term. In both classical and quantum mechanical perspectives, the resonant condition between the sites disappears. In classical mechanics, the energy does not transfer onto the other oscillator. In quantum mechanics, there is energy transfer due to tunneling but only to the same energy levels on the other oscillator.

For our calculations, the Hamiltonian is best represented in the occupational basis set of harmonic oscillators, also known as Fock states. The occupational basis set is a direct product of the occupations of all oscillators: $|N_1N_2\cdots N_i\rangle$, where N_i is the occupational state on the i^{th} oscillator. For our calculations, i=2. The Hamiltonian of the system in terms of creation and annihilation operators of the 1D harmonic oscillators is given as:

$$H = c_h * H_h + c_a * H_a + c_c * H_c (2)$$

$$H_h = \sum_{i} a_i^{\dagger} a_i + a_i a_i^{\dagger} \tag{3}$$

$$H_a = \sum_{i} a_i a_i a_i a_i + a_i a_i a_i^{\dagger} + a_i a_i a_i^{\dagger} a_i + \dots + a_i^{\dagger} a_i^{\dagger} a_i^{\dagger} a_i^{\dagger}$$

$$\tag{4}$$

$$H_c = \sum_{i}^{\dagger} \left(a_i a_{i+1} + a_i a_{i+1}^{\dagger} + a_i^{\dagger} a_{i+1} + a_i^{\dagger} a_{i+1}^{\dagger} + \dots + a_{i+1}^{\dagger} a_i^{\dagger} \right)$$
 (5)

 $c_h = 1.0$, c_a is a coefficient for anharmonicity in the system (for example $c_a = 0.02$ in most of our calculations) and c_c is a coefficient for coupling between the oscillators.

The number of levels in the basis set and the size of the matrix required for the calculation depend on the displacement of the coherent state and anharmonicity of the system. At the higher energy, where the overlap between initial state and eigenstates is small, the basis set is truncated. For example, truncating as early as 10 occupational states on each site is enough for the displacement of 1.0 a.u. and $c_a < 0.05$. The total dimensionality is the number of states of a single oscillator to the power of the number of the oscillators.

We choose a coherent state as an initial state because it helps to bridge the gap between understanding physics in the classical and quantum limits and it helps to bring the theory closer to the experiment by using coherent state base methods. A coherent state is a state of a minimum uncertainty [26]. In the basis set of occupational eigenstates of the harmonic oscillator $|i\rangle$, a coherent state of a single site takes the form of Eq.7 [26].

$$|\alpha(x_0)\rangle = \sum_{i} c_i(x_0)|i\rangle,$$

$$c_i(x_0) = e^{-\frac{|x_0|^2}{2}} \frac{|x_0|^i}{i!},$$
(6)

where $c_i(x_0)$ represents the contribution from the i^{th} energy level and x_0 is the displacement of the coherent state. Our basis set is a direct product of occupational states of two harmonic oscillators.

$$|\psi(\mathbf{x_0})\rangle = \sum_{i,j} c_i(x_{0i})c_j(x_{0j})|ij\rangle$$

$$c_i(x_{0i}) = e^{-\frac{|x_{0i}|^2}{2}} \frac{|x_{0i}|^i}{i!}$$

$$c_j(x_{0j}) = e^{-\frac{|x_{0j}|^2}{2}} \frac{|x_{0j}|^j}{j!}$$
(7)

To resemble the transfer of energy in classical dynamics, the coherent state is displaced on only one of the oscillators. Now that we have defined the initial state and know the eigenstates of the system, we can observe the dynamics.

The spectrum represents the dynamics of the system in the frequency domain. The spectrum of a quantum system consists of discrete energy values. These energy values are found by diagonalization of the Hamiltonian. For diagonalization, we use the symmetric QR routine from GMM++ library (an interface to LAPACK), which produces the eigenvalues

and eigenvectors of the system. The intensity of the spectral lines depends on the initial state. One can either do a Fourier transform of the auto-correlation function or write an initial state in the eigenstate basis. We use the second approach. We find the intensity of the eigenvalue's peak by taking a normalized dot product between the initial state and the corresponding eigenstate (Eq.8).

$$c_k^{initial} = c_k^{final} = \frac{\langle \psi_{initial} | e_k \rangle}{\langle \psi_{initial} | \psi_{initial} \rangle}, \tag{8}$$

where $|e_k\rangle$ is the i^{th} eigenstate.

To view the dynamics in the time domain, we compute the auto-correlation function, which is a projection of the initial state onto the final one, $(\langle \psi_{final} | \psi_{initial} \rangle)$. To get the final state from the initial one, we need to use a time-propagation operator $e^{-i\hat{H}t}$. To do that, we expand the initial state in terms of eigenstates. Eq. 9 expresses the auto-correlation function in terms of the eigenstates and coefficients c_k , which are a projection of the initial state onto the eigenstates (Eq. 8).

$$\langle \psi_t | \psi_0 \rangle = \sum_k |c_k|^2 e^{-iE_k t} \tag{9}$$

III. RESULTS

A. Tunneling and non-tunneling modes

Signatures of breathers can be observed in the spectrum of the system. In the spectrum, we would like to distinguish two types of modes: non-tunneling and tunneling modes. Tunneling modes arise when the coupling between the oscillators is not strong enough to create an eigenstate, where the wave function density is shared between the sites – the particle has to tunnel from one site to the other. In a classical limit, the tunneling time approaches infinity and these tunneling modes become DB modes. When there is a considerable amount of shared wave-function density between the sites, an alternative type of modes manifests – non-tunneling modes. These modes can be seen clearly in a low energy region, where coupling dominates. Besides limiting cases, where there is either a small or large amount of shred density between the sites, it is sometimes hard to distinguish between tunneling and non-tunneling modes. In the following sections we show that the transition between these two types of modes is smooth. To have a better understanding of how the two coexist in

the same energy region, let us first focus on the limiting cases: coupled harmonic oscillators with no anharmonicity (Fig. 1 (top)) and anharmonic oscillators with no coupling (Fig. 1 (middle)). We then analyze the case where the potential combines both anharmonicity and coupling (Fig. 1 (bottom)).

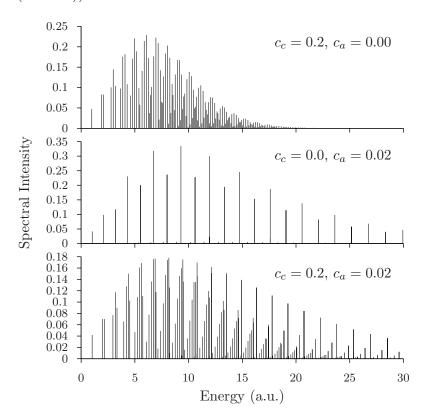


FIG. 1: Spectrum of a coherent state in a system with the Hamiltonian in Eq.1. The **top** panel is the harmonic limit $(c_a = 0)$. All of the spectral lines are non-tunneling modes. The spectral lines in the **middle** panel are tunneling modes — the anharmonic limit $(c_c = 0)$. The **bottom** panel shows modes in a coupled anharmonic potential. The spectrum (bottom) has modes that resemble both limiting cases (top and middle). The modes that resemble the delocalized modes are non-tunneling modes and the modes that resemble the localized modes are tunneling modes.

In the coupled case (Fig. 1 (top)), we see a splitting of the energy levels. All of the eigenstates in this case are non-tunneling. For example, at 2 a.u., a system of uncoupled harmonic oscillator would have the second lowest eigenstate $|1\rangle$. Since there is a coupling between the oscillators, these $|1\rangle$ states of each oscillator combine into a linear combination of symmetric and anti-symmetric states: $|10\rangle + |01\rangle$ and $|10\rangle - |01\rangle$. For the third lowest

states ($|02\rangle$, $2 \times |11\rangle$ and $|02\rangle$), we also see splitting around the energy of $|2\rangle$ of a system of uncoupled harmonic oscillator at 3 a.u. For each eigenvalue of a 1D oscillator, in the case of coupled oscillators, we get a group of states. Each state in that group is a linear combination of states that have the same energy; for example, $|05\rangle$, $|14\rangle$, $|23\rangle$, $|32\rangle$, $|41\rangle$ and $|50\rangle$. This is an example of what we call same-quanta group – a group of states that have the same energy. We extend this definition to non-linear cases by defining same-quanta group as a group of states that become degenerate when non-linearities of the potential are decreased to zero.

The other limiting case is when there is anharmonicity and no coupling (Fig. 1 (middle)). The spectrum is similar to that of a 1D oscillator. There is no splitting between the states of the different sites. The ground state energy is at 1 a.u.; this is because there are two oscillators with energy ≈ 0.5 a.u. for each. Since there is no coupling, all of the modes on the graph (Fig. 1 (middle)) are tunneling modes in the limit of tunneling time being infinity.

In a coupled harmonic case, the levels split due to coupling. A similar situation occurs in the case of coupled anharmonic potential. Once there is a coupling between tunneling modes, they split. The difference is that in the anharmonic case only two states can be involved in splitting; for example, $|90\rangle$ and $|09\rangle$ are involved and $|81\rangle$, $|72\rangle$, $|63\rangle$, ..., $|18\rangle$ are not involved in the same splitting. In the harmonic coupled case, all of the levels with the same number of quanta split together.

The system that includes both coupling and anharmonicity (Fig. 1 (bottom)) resembles both limiting cases: $c_a = 0$ (Fig. 1 (top)) and $c_c = 0$ (Fig. 1 (middle)). At lower energy, the non-tunneling modes dominate and at higher energy, tunneling modes dominate. A classical mechanical description of DBs separates localized and delocalized modes' energy regimes by separatrix. Our analysis of the eigenstates contour plots shows that, from a quantum mechanical perspective, non-tunneling modes, the quantum equivalent of delocalized modes, can be found higher in the energy spectrum. There is also no clear separation between regions with non-tunneling and tunneling modes. As energy increases, tunneling modes slowly emerge out of non-tunneling modes that are lower in energy. This region in energy, where both tunneling and non-tunneling modes can be found, we define as a transient region (Fig. 1 (bottom), a region of 10-15 a.u.). The tunneling modes manifest as isolated peaks that resemble the modes in uncoupled quartic potential. At the energy higher than the transient region, they can be seen clearly. The contour plot analysis shows that the wave

function of the tunneling modes is localized on the sites. These modes are equivalent to localized modes in a classical mechanical description of DBs. The non-tunneling modes resemble the modes in coupled harmonic potential. They have a significant wave-function density between the sites and appear lower in energy where non-linear contributions are not significant. The non-tunneling modes are an equivalent of delocalized modes in classical mechanics description of DBs.

We deliberately choose the values for the c_a and c_c coefficients and the position of the coherent state on site 1 (q_1) . The intention is to clearly show a transient region and the interplay between the non-tunneling and tunneling modes. Not many natural systems have an initial state that spans over such a large number of states. For example, in C-H, stretch anharmonicity dominates the coupling already in the second excited state [27]. However, our choice of the system parameters and initial conditions gives a general understanding of the dynamics. In heavy oscillators, such as nano-mechanical cantilever arrays or large molecules with hydrogen bonding, the displaced state can spans over a large number of states, which would be similar to our model.

The spectrum shows the overlap of the initial state with eigenstates. Let us understand the mechanism that develops this spectrum. The intensity is a projection of an initial state on eigenstates. The more similar the distribution of the wave-function between initial state and eigenstate, the higher the intensity at the corresponding eigenvalue. For example, at low energy and at the very high energy of the spectrum, the initial state does not have much density; therefore, we do not see much intensity. The majority of intense states are at the energy $H(q_1 = 3.5, q_2 = 0.0)$. If only one of the oscillators has a displaced state and the other one does not, the initial state contour plot has non-zero elements only along one of the axes. Non-tunneling eigenstates at lower energy have a considerable amount of density that overlaps with non-zero elements of the coherent state. At higher energy, anharmonicity prevails and the tunneling eigenstates have a considerable overlap with the initial state. The wave-function of tunneling eigenstates concentrates on the oscillators instead of being shared between them. These tunneling eigenstates correspond to the highest energy states from the group of states that came from single level of uncoupled oscillator. Since our initial state has dominant population on the oscillators and not shared between them, the eigenstates that have density localized on oscillators, have higher intensity.

Contour plots of eigenstates show the energy distribution within an eigenstate. Quantum

dynamics of the coherent state (Fig. 1 (bottom)) result from the projection of the initial state onto the eigenstates. By visualizing and comparing the density distribution of initial wave function and eigenstates, one can understand how the spectrum forms. For example, the wave-function of tunneling eigenstates has higher density concentrating on the sites; it can be seen as higher overlap with $|i,j\rangle$ states where $|i-j|\approx i+j$. Therefore, the initial state, which is localized on sites rather than delocalized between the sites, will have a higher intensity.

2D contour plots of eigenstates' wave function visualize how the probability density distributes among the oscillators. The procedure for getting these contour plots is the following. The Hamiltonian matrix is written in the Fock basis, which is a direct product of occupational states of each oscillator. The matrix is diagonalized. The eigenstates that are in the Fock basis are rewritten as a 2D matrix. The columns of the matrix are enumerated according to the Fock states of the first oscillators: $|0,i\rangle, |1,i\rangle, \ldots, |n,i\rangle$; where $i = 0 \cdots n$. The rows are enumerated according to the Fock states of the second oscillator: $|i,0\rangle, |i,1\rangle, \ldots, |i,n\rangle$. And the elements of the matrix are elements of the eigenstate that is written as a 2D matrix. The contour plots show these matrices. A value at a coordinate (x,y) corresponds to a component of $|x,y\rangle$ basis vector. Fig. 2 gives an example of such contour plot. The figure also explains how to interpret the plot in terms of the occupational levels of the harmonic oscillators.

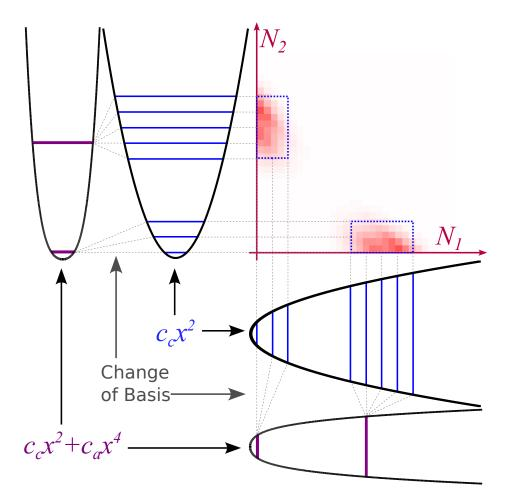


FIG. 2: (Color online) The schematic shows how to interpret a contour plot of an eigenstate. Each axis represents Fock states for each site's harmonic oscillator $(c_c x_i^2)$. The value on the axis is the eigenvalue of the harmonic oscillator Fock state. The schematics shows that to portray the calculated eigenstate, we need to change the basis set from anharmonic $(c_c x_i^2 + c_a x_i^4)$ to the harmonic $(c_c x_i^2)$ one. Due to this representation of the eigenstate, we can distinguish the tunneling mode by identifying that localization of the wave-function (red) is towards the axis.

These plots help to visualize and distinguish localized from delocalized states. There are other benefits, too. The contour plots of the eigenstates are well suited to illustrate the transition between localized and delocalized modes and identify modes that have signatures of both. We will also describe the origin of the higher order breathers, the small satellite peaks that are a little lower in energy then localized modes on Fig. 1 (bottom).

Fig. 3 shows examples of tunneling (d, e) and non-tunneling modes (a,b,c). Tunneling

mode contour plots show a non-zero density next to the axis, where the value on one axis is high and on the other axis is low. This density distribution shows that one of the oscillator is in the lower modes and the other one is in the higher ones. Another way to distinguish the tunneling modes is to see that the value of the plotted eigenstate along the rising diagonal is close to zero. Non-tunneling modes, on the other hand, have values of wave-function concentration on the increasing diagonals, meaning the eigenstate wave-function is shared between both sites.

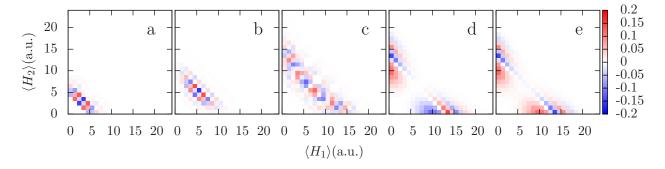


FIG. 3: (Color online) Plots **a**, **b** and **c** are examples of non-tunneling modes. They correspond to 21st (with the energy 7.1494 a.u.), 50th (11.6861 a.u.) and 95th (16.3442 a.u.) energy levels. **d** and **e** plots are examples of tunneling modes. They are quantum equivalent of classical breathers. The two shown plots are anti-symmetric and symmetric states corresponding to 93rd (16.3329 a.u.) and 94th (16.3332 a.u.) energy levels respectively.

The wave-function value between non-tunneling and tunneling eigenstates oscillates differently along the decreasing diagonal – the line connecting $|0,n\rangle$ and $|n,0\rangle$. In tunneling modes, the wave function either does not change sign at all along the decreasing diagonal for the symmetric case, or changes the sign only once for the anti-symmetric case. In the tunneling modes, the wave function varies slightly. In non-tunneling modes on the other hand, the wave function quickly varies, which is seen as blue and yellow peaks alternating along the diagonal.

In more detail, the contour plot of the tunneling modes (Fig. 3 (d,e)) correspond to the pair of peaks at 16.33 found in the spectrum plot (Fig. 1 (bottom)). The pair appears as a single peak; two states are only 0.003 a.u. apart. The eigenstate that is higher in energy is symmetric and the lower one is anti-symmetric. The small splitting between symmetric and anti-symmetric states of the tunneling modes pair is consistent with classical formulation of

DBs.

Tunneling modes become breather modes in the classical limit $(xp \gg \hbar)$. An important observation is that the distribution of absolute wave-function is very similar in the pair but one state is symmetric and the other one is anti-symmetric. From these two observations an important similarity to the classical mechanical view can be concluded. If both states are occupied, then the density on one of the oscillators cancels out. However, because these have different energies, they evolve in time with different periods and at some point there will be more energy on the other oscillator. This contradicts the classical behavior of breathers. However, the splitting is very small and therefore the time of the transfer is very long.

Illustrating the intensity and distribution of energy we understand how the energy is distributed between the sites. This allows us to study in detail the transient region, the variation of coupling, the influence of initial displacement and the higher order tunneling modes. Contour plots proved to be an important tool to distinguish between localized and delocalized modes. They would be even more important when the density of states increases and the spectrum becomes complex; for example, in soft potentials or when $xp \gg \hbar$. Furthermore, contour plots help us to understand the evolution of non-tunneling into tunneling modes.

B. Transient Region

Most of the potentials in nature are non-linear and have localized modes when the energy is high enough. At lower energies the non-linear potential can be approximated by linear ones. This approximation is similar to the sine approximation for the motion of a pendulum that one learns in an introductory physics classes. With an increase in energy, the non-linearity becomes more important and the system dynamics changes from delocalized modes to localized modes. The transition is important because the behavior of the system changes significantly. In the delocalized mode regime, the system transfers the energy from one site onto the next one but in the localized modes regime the energy is localized in the classical limit and takes almost infinite time to transfer in the quantum limit. We model this transition in the simplest potential – two coupled quartic oscillators. In other potentials the transition might be quantitatively different but conceptually the same.

The transition from the non-tunneling modes region to the tunneling modes region has

a different mechanism in classical and quantum mechanics. In classical mechanics the two regions are divided by a separatrix. In contrast, quantum mechanics cannot have such a sharp division. The energy, in quantum mechanics, does not localize – it takes an almost infinite amount of time to transfer through tunneling. Therefore, in contrast to classical mechanics, tunneling modes slowly evolve from the non-tunneling modes as energy increases. Understanding the quantum equivalent for the transition from delocalized to localized modes will help to understand the limitations of a classical model, while providing insight into semi-classical dynamics, and complimenting experiments on QDBs.

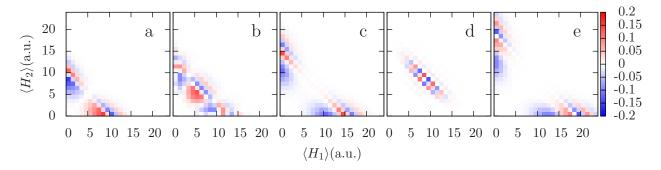


FIG. 4: (Color online) Contour plots (see Fig. 2) of delocalized (\mathbf{b} , \mathbf{d}) and tunneling (\mathbf{a} , \mathbf{c} , \mathbf{e}) modes within the transient region (12-23 a.u.). The plots are in the order of increasing energy: plot \mathbf{a} is 55th state with the energy 12.1386, \mathbf{b} – 75th – 14.454, \mathbf{c} – 110th –17.7796, \mathbf{d} –145th – 20.82 and \mathbf{e} – 163 – 22.2542. The figure shows that in the transient region, the tunneling and the non-tunneling modes alternate.

Depending on the system's Hamiltonian and the initial conditions, transient region can contain part or all of the coherent state. There, non-tunneling and tunneling modes co-exist. Fig. 1 (bottom) shows that they alternate with an increase in energy. Tunneling modes are the highest energy modes from the same-quanta group. The transient region may contain a number of same-quanta group. It can also contain non-tunneling states followed by the tunneling states of the same-quanta group, further followed by non-tunneling states and tunneling states of the next same-quanta group. Fig. 4 gives an example of alternating tunneling and non-tunneling modes.

In classical mechanics, the transition from localized to delocalized modes is a stepfunction. Fig. 5 shows highest energy eigenstates from the same-quanta groups within the transient region. Here one can observe an iterative transformation from non-tunneling to tunneling modes. This quantum in nature phenomenon significantly contrasts with the step transition from delocalized to localized modes in classical mechanics.

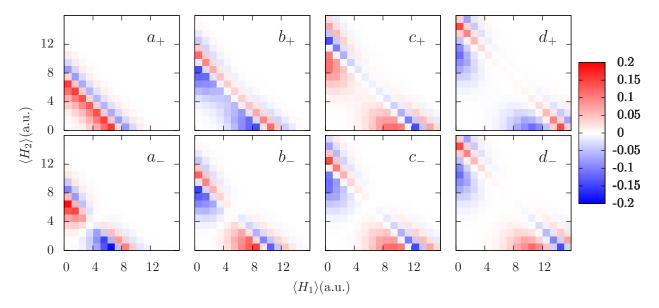


FIG. 5: (Color online) Smooth transition from non-tunneling modes (a) into tunneling modes (d). Vertical pairs of plots show symmetric (+) and anti-symmetric (-) eigenstates. From the same-quanta group, these states have the highest localization. As the energy of the states increases ($\mathbf{a} \to \mathbf{d}$), the wave-function moves towards the axis. The presence of the wave-function between the axis, which corresponds to the density between the sites, gradually decreases; \mathbf{d} has negligible amount of wave-function between the sites – the wave function hast to tunnel from one site to the other. The corresponding values of energy (E) and intensity (I) for the plots are: a_+) E=9.46539 E=0.175297, a_-) E=9.50399 E=0.135935, b_+) E=12.1386 E=0.161693, b_-) E=12.1478 E=0.151122, c_+) E=14.9101 E=0.139205, c_-) E=14.9113 E=0.138124, d_+) E=17.7795 E=0.11148 and d_-) E=17.7796 E=0.111422.

Unlike in a classical mechanical perspective, the transition to tunneling modes from nontunneling modes is smooth and there is no distinct separatrix as in the classical case. Fig. 5 shows this transition. The last two plots on the right $(d_- \text{ and } d_+)$ are clearly tunneling modes; there is no shared density between the sites and the wave-function has to tunnel through. The majority of contribution to these eigenstates comes from basis states that have excitation only on one of the sites; for example, $|14,0\rangle$ and $|0,14\rangle$. The two plots on the left of Fig. 5 $(a_- \text{ and } a_+)$ are a pair of eigenstates that resemble the tunneling mode. The pair of states, b_{-} and b_{+} (Fig. 5) has features similar to the tunneling modes, it is more delocalized than the tunneling mode since there is a significant amount of density on the increasing diagonal, meaning that there is overlap with basis states that have density delocalized between the sites. The pair in the middle is between two cases. We can see the development of a localized state.

C. Additional observations

1. Variation of the Coupling

Slight changes in the setup of an experiment can vary the shape of the potential. For example, one can change parts of the molecules to be heavier or lighter, or use a different kind of a solution. These kind of slight changes can control the interplay between the non-linearity and coupling in the potential.

From Fig. 1, we are familiar with signatures of breathers in a spectrum. We extend those results by investigating not only how they appear but also how they depend on the parameters of the potential. We analyze the evolution of the eigenvalues with respect to coupling coefficients in the Hamiltonian (Eq.1). We start from zero coupling ($c_c = 0$) and increase it to the point where coupling is much larger than anharmonicity, where the spectrum would resemble the harmonic coupled spectrum. We focus on eigenvalues of the same-quanta group of states and print the eigenvalues between 9.1 and 11.4. The coefficient of anharmonicity is constant: $c_a = 0.02$.

Fig. 6 shows dependence of eigenvalues of anharmonic oscillators on coupling (c_c) . The plot shows variation of eigenvalues from one extreme of two uncoupled anharmonic oscillators $(c_c = 0.0)$ to another that has coupling $(c_c = 0.3)$ much larger than anharmonicity $(c_a = 0.02)$. With this plot, we would like to focus on a group of same-quanta states. At $c_c = 0$, the eigenstates of that group have energy in the interval $\approx (10, 10.6)$ a.u. The figure clearly shows how increase in coupling causes degenerate states to split. The tunneling states, which are the top states of the same-quanta group, are the last ones to split. Keeping in mind that the size of splitting is inversely proportional to the transfer time between the sites and noting that tunneling state approaches a similar size of splitting as lower-lying non-tunneling modes, one can conclude that in a quantum mechanical perspective the transition

from tunneling to non-tunneling states is smooth. This observation compliments our result in section IIIB on the smooth transition between tunneling and non-tunneling modes.

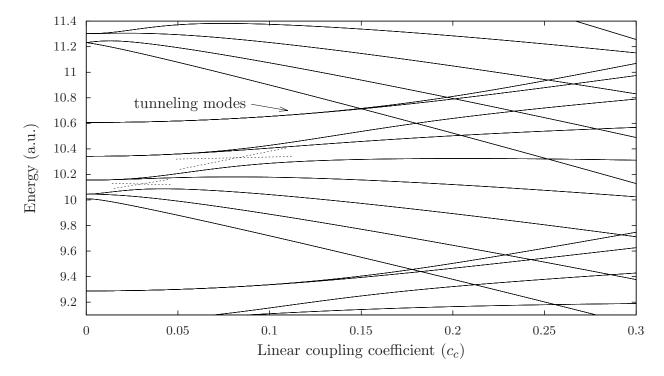


FIG. 6: Eigen energy of quartic dimer (Eq. 1) with $c_h = 0.5$ and $c_a = 0.02$. Dashed crossing lines indicate examples of the avoided crossings.

We observe avoided crossing for the states from the same-quanta group. At $c_c \approx 0.8$, the top (symmetric) state that starts at ≈ 10.34 avoids crossing with the low state that starts at ≈ 10.14 . Another avoided crossing happened at $c_c \approx 0.04$ for the next lower pair of states. In harmonic case, there is no crossing since the degenerate states split linearly and do not cross. Previously, avoided crossing was observed in anharmonic trimer [23]. The avoided crossing is expected since the eigenstates belong to the same symmetry group of irreducible representations. The practical importance of this result would show up in systems with many degrees of freedom. In multidimensional systems, the avoided crossings become conical intersections that allow for radiation-less transition between the energy surfaces [28].

2. Higher Order tunneling modes

In the spectrum plots (Fig. 1), one can notice that besides tunneling modes, there are eigenstates of considerable intensity in the anharmonic regime, where there are no non-tunneling modes – the energy region beyond 16 a.u. (Fig. 1 (bottom)). These eigenstates do not classify as non-tunneling modes. In this higher energy regime the influence of coupling is small, and contrary to non-tunneling modes, they increase in intensity with increase in energy. Furthermore, they also do not belong to our previous definition of tunneling modes. They do not have highest intensity of the same-quanta group in the anharmonic energy regime and they are not a linear combination of modes that have a ground state on one of the sites and occupy high state of the other site.

The anomaly becomes clear when we analyze at the contour plots of these eigenstates (Fig. 7). In these eigenstates, the energy has to tunnel from one site to the other; it is similar to the tunneling eigenstates. The contour plots evidence a distinction of these eigenstates from tunneling modes – the majority of the wave function density is not on the axis. These two observations motivate us to define them as higher order tunneling modes (HOTM). Fig. 7, specifically, is an example of second order tunneling modes (SOTM). In the basis set of a direct product of anharmonic oscillators, they are a linear combination of $|n-1,1\rangle$ and $|1,n-1\rangle$ states. Fig 1 shows other HOTM that are even smaller in intensity than SOTM and manifest at even higher energy limit. Next, we compare HOTM and first order tunneling modes and outline a couple of other interesting points.

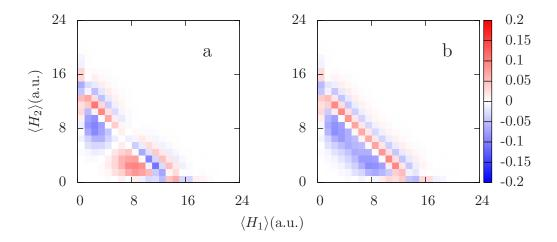


FIG. 7: (Color online) An example of higher order tunneling modes, specifically the second order tunneling modes. Contour plots of 90th (E=16.01) and 91th (E=16.05) energy levels.

To identify the relation of HOTM to tunneling modes, we would like to point out few similarities. As seen from Fig. 7, HOTM are a pair of symmetric and anti-symmetric states with a higher probability of being on the oscillators rather then shared. On the figures, one can see the lack of density on the increasing diagonal; the density closer to axis. As seen in Fig. 6 at the energy 10.33 a.u., HOTM start as degenerate states but further along, they split into a pair, similarly to the first order tunneling states. Since we are looking at lower value of coupling, we can see HOTM at 10.33, rather than at 16 a.u.

To emphasize that HOTM should be treated different from the first order tunneling modes, we would like to point out some key differences. The probability density in HOTM shifts towards the other oscillator by one occupational level. Fig. 7 shows this shift in density for the second order tunneling modes; they correspond to $|n-1,1\rangle$ and $|1,n-1\rangle$ occupational states. The maximums of the wave-functions are not on the axes anymore but are closer to the increasing diagonal. Comparing to the energy region 10.3-10.6 a.u. of the tunneling modes in Fig. 6, the SOTM have larger splitting between symmetric and antisymmetric modes than the first order ones. The distance between the top left and bottom right density concentrations in the contour plot is related to the tunneling probability; therefore, it is rational to assume that with decrease of this distance the splitting and the tunneling probability increases.

3. Influence of the Initial Displacement

Initial state determines the intensities in the spectrum. We show that when initially both of the sites are displaced, HOTM have higher intensity than tunneling or non-tunneling modes. The impact of this observation is twofold: we gain insight on experiments with displaced coherent states on all sites and we understand influence of HOTM in the dynamics. Depending on the experimental system setup, the initial conditions can be different. When experimental setup cannot target a specific site, multiple sites will be displaced. An example of this would be exciting a number of sites in a system from a ground state to an excited state, where the excited state is displaced. One application may be understanding of DNA breaking under THz radiation [29]. Emphasizing presence of the HOTM in the dynamics, on the other hand, results in a new type of dynamics – the energy is neither localized on sites nor distributed between the sites.

Fig. 8 illustrates the effects of displacing the coherent states symmetrically on both sites (the bottom panel), in contrast to displacing on just one of the sites (the top panel). In the lower energy region (< 6 a.u.), the effect of displacing both sites is clear. At 2 a.u. for example, the case with both sites displaced (BSD) has only one line corresponding to a symmetric eigenstate; the case with one site displaced (OSD) has both symmetric and anti-symmetric modes. In case of BSD, the pattern continues at higher energies – only the symmetric eigenstates have intensity. Furthermore, in the same-quanta group the highest energy eigenstate have the highest intensity. In the transient region (10-15 a.u.), SOTM start to get priority. The OSD case has an opposite trend. At lower energies, middle of the same-quanta group has the highest intensity. In the transient region, tunneling modes start to dominate. However, the most interesting contrast is in the anharmonic region, where in OSD case, tunneling modes dominate. In BSD, SOTM and other HOTM dominate.

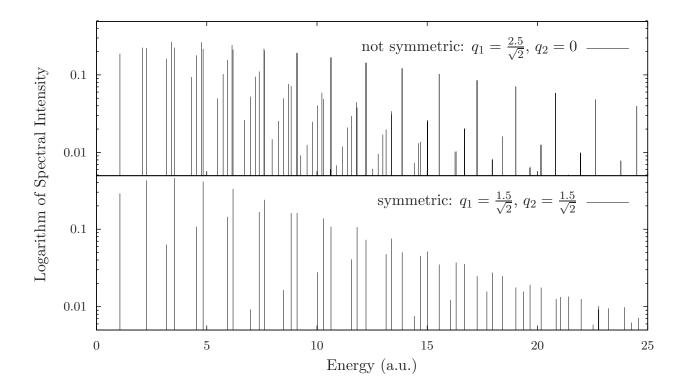


FIG. 8: The **top** plot is a spectrum from Fig. 9 with a log scale. The **bottom** plot is the same as the top plot but for different initial conditions – both of the sites have symmetrically displaced coherent state.

In classical mechanics if both sites have the same amount of the initial energy, there is no transfer of energy. In quantum mechanics on the other hand, coherent state is a superposition of eigenstates – the dynamics is more complex. To get a brief understanding, let us analyze the dynamics around 20 a.u. In the case of OSD, the tunneling mode pair has most of the intensity. As we mentioned earlier, the energy transferred from one site to the other. In the case of BSD, the intensity is distributed only among the symmetric modes – there is no transfer of energy between the sites. However, the energy is distributed almost evenly among HOTM. HOTM have some density shared between the sites. With time, the density oscillates from being localized on sites to being partially shared between the sites.

4. Autocorrelation of the displaced coherent state

A number of time-domain methods are based on propagation of a coherent states. Examples include HK [14], QHD [13], CSPI [20], CCS [17] and MP-SOFT [18, 19]. Earlier we

calculated eigenstates to analyze dynamic properties of the system. Eigenstates represent stationary properties of dynamics. To compare our results to time-domain methods, we calculate auto-correlation function. Besides showing evolution of the initial state in time, auto-correlation function is used to calculate spectroscopically properties, diffusion rate, and reaction rate constants. Fig. 9 shows auto-correlation function (Eq.9) for different values of anharmonicity in the potential Eq.(5). The system is the same as in Fig. 1 with $c_c = 0.2$.

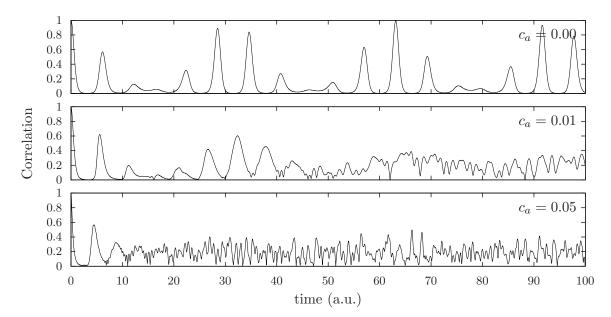


FIG. 9: Auto-correlation functions $\langle \phi(t)|\phi(0)\rangle$ for different value of anharmonicity coefficient c_a : $c_a=0.00$ (top), $c_a=0.01$ (center) and $c_a=0.05$ (bottom). The effects of increasing the anharmonicity and loss of resonance can be seen as c_a increases. In all cases the wave packet on the first oscillator is displaced to $x_0=1.767$.

The top panel shows a dynamics of coupled harmonic oscillators. The wave-function comes back to the previous state with a period of 65 a.u. Once there is anharmonicity $(c_c = 0.01, \text{ middle panel})$, the eigenstates have frequencies that are not multiple of each other anymore. The condition for resonance is lost, and the tails of coherent state move at different frequencies. The coherent state spreads with time. The wave function does not come back to the same state. The case with $c_a = 0.05$ (bottom panel) is an even more extreme example. The coherent state spread even faster. Calculating rapidly spreading coherent state is difficult. This result shows the challenge that coherent state based pathintegral methods have to face – they have to track quickly spreading tails of the coherent

state. Nevertheless, the time-window that we used proves to be sufficiently large to get satisfying results. In addition, quick decrease of auto-correlation function in time justifies using shorter propagation times. Time-domain methods that are based on propagation of coherent state will prove to be an effective and accurate tool to model signatures of QDBs in multidimensional systems.

IV. DISCUSSION AND CONCLUSIONS

Understanding signatures of QDBs in the quantum dynamics of coherent states is a step towards applying the localization phenomenon to large scale systems and bridging the gap between concepts of quantum and classical DBs. We identified and analyzed tunneling modes, a quantum counterpart of classical DBs, in the spectrum of quartic dimer using contour plots. Further, we visualized the eigenstates within transient region. In contrast to the behavior of classical breathers, a transition from non-tunneling modes to tunneling modes is gradual and smooth. We also presented additional important observations: tunneling modes avoid crossing with non-tunneling modes from the same-quanta group; new types of modes, HOTM appears at higher energies; controlling initial conditions allow us to prioritizes HOTM in the spectrum; auto-correlation function decay faster with increase in non-linearity, which shortens a required time for calculation.

Tying our results to classical mechanical interpretation of DBs, we show that tunneling and non-tunneling modes are the quantum mechanical counter part of localized and delocalized modes that appear in classical mechanics. Since coherent states span a large number of eigenstates, they simultaneously contain both tunneling and non-tunneling modes. In the classical mechanic analogue, the initial energy localized on one of the sites, cannot completely transfer to the other site. In quantum mechanics, the energy tunnels to the other site; however, as the size of the system approaches a classical limit, the tunneling time approaches infinity.

From the analysis of the transient region, we concluded that tunneling and non-tunneling modes alternate with increasing energy, and that the transition from non-tunneling to tunneling modes is smooth. Both of these conclusions are in contrast with the classical mechanical model of breathers, where localized and non-local modes are separated sharply at a certain energy. The convergence of the transient region in quantum mechanics to the separatrix

point in classical mechanics can be possibly reached by scaling the quantum result to the classical limit.

Many semi-classical methods that are capable of approaching large systems rely on propagation of coherent state. We show that both tunneling and non-tunneling modes are present in the coherent state. Therefore part of the coherent state would stay localized and part would be delocalized. The CSPI methods would have difficulty tracing the width or other metrics of the coherent state, especially in the transient region, where both types of states have a close to equal contribution. Nevertheless, CSPI methods should be able to identity the location of the transient region.

Acknowledgments

The research was funded by the NSF grant CHE-1050405 and NSF CAREER Award No. 0645340.

- P. Maniadis, B. S. Alexandrov, A. R. Bishop, and K. O. Rasmussen, Phys. Rev. E 83, 011904 (Jan 2011)
- [2] G. T. Adamashvili, C. Weber, A. Knorr, and N. T. Adamashvili, Phys. Rev. A 75, 063808 (Jun 2007)
- [3] M. Sato, B. E. Hubbard, A. J. Sievers, B. Ilic, D. A. Czaplewski, and H. G. Craighead, Phys. Rev. Lett. 90, 044102 (Jan 2003)
- [4] M. E. Manley, A. J. Sievers, J. W. Lynn, S. A. Kiselev, N. I. Agladze, Y. Chen, A. Llobet, and A. Alatas, Phys. Rev. B 79, 134304 (Apr 2009)
- [5] P. Binder, D. Abraimov, A. V. Ustinov, S. Flach, and Y. Zolotaryuk, Phys. Rev. Lett. 84, 745 (Jan 2000)
- [6] B. I. Swanson, J. A. Brozik, S. P. Love, G. F. Strouse, A. P. Shreve, A. R. Bishop, W.-Z. Wang, and M. I. Salkola, Phys. Rev. Lett. 82, 3288 (Apr 1999)
- [7] B. Eiermann, T. Anker, M. Albiez, M. Taglieber, P. Treutlein, K.-P. Marzlin, and M. K. Oberthaler, Phys. Rev. Lett. 92, 230401 (Jun 2004)
- [8] S. Aubry, Physica D: Nonlinear Phenomena 103, 201 (1997)

- [9] O. Bohigas, S. Tomsovic, and D. Ullmo, Physics Reports 223, 43 (1993), ISSN 0370-1573, http://www.sciencedirect.com/science/article/B6TVP-46SXP1D-1G/2/b4f28807ad6f8b3b3059b8b51f
- [10] S. Pnevmatikos, A. V. Savin, A. V. Zolotaryuk, Y. S. Kivshar, and M. J. Velgakis, Phys. Rev. A 43, 5518 (May 1991)
- [11] Y. Kinoshita, Y. Yamayose, Y. Doi, A. Nakatani, and T. Kitamura, Phys. Rev. B 77, 024307 (Jan 2008)
- [12] A. V. Savin and Y. S. Kivshar, Phys. Rev. B 81, 165418 (Apr 2010)
- [13] O. V. Prezhdo and Y. V. Pereverzev, The Journal of Chemical Physics 116, 4450 (2002), http://link.aip.org/link/?JCP/116/4450/1
- [14] M. F. Herman and E. Kluk, Chemical Physics 91, 27 (1984), ISSN 0301-0104, http://www.sciencedirect.com/science/article/B6TFM-44X7T6B-6D/2/08f4d4ea45d3ea4a3bbc1593f1
- [15] G. Hochman and K. G. Kay, The Journal of Chemical Physics 130, 061104 (2009), http://link.aip.org/link/?JCP/130/061104/1
- 0301-0104, [16] K. G. Kay, Chemical Physics **322**, (2006),ISSN 3 real-time dynamics complex honour Phil quantum systems in Pechukas, http://www.sciencedirect.com/science/article/B6TFM-4GMGWK5-7/2/aa1dcdca71031b35a36ede70aef
- [17] D. V. Shalashilin, The Journal of Chemical Physics 132, 244111 (2010), http://link.aip.org/link/?JCP/132/244111/1
- [18] Y. Wu and V. S. Batista, The Journal of Chemical Physics 121, 1676 (2004), http://link.aip.org/link/?JCP/121/1676/1
- [19] Y. Wu and V. S. Batista, The Journal of Chemical Physics 118, 6720 (2003), http://link.aip.org/link/?JCP/118/6720/1
- [20] A. D. Ribeiro, M. A. M. de Aguiar, and M. Baranger, Phys. Rev. E 69, 066204 (Jun 2004)
- [21] K. Igumenshchev and O. Prezhdo, Phys. Rev. E(accepted)
- [22] V. Fleurov, R. Schilling, and S. Flach, Phys. Rev. E 58, 339 (Jul 1998)
- [23] S. Flach and V. Fleurov, Journal of Physics: Condensed Matter 9, 7039 (1997), http://stacks.iop.org/0953-8984/9/i=33/a=007
- [24] S. Aubry, S. Flach, K. Kladko, and E. Olbrich, Phys. Rev. Lett. 76, 1607 (Mar 1996)
- [25] K. Igumenshchev and M. Ovchinnikov(in progress)
- [26] L. Landau and E. Lifshitz, Quantum mechanics: non-relativistic theory, Teoreticheskaia fizika (Izd. 3-e) (Landau, L. D, 1908-1968) (Butterworth-Heinemann, 1991) ISBN 9780750635394,

- http://books.google.com/books?id=J9ui6KwC4mMC
- [27] R. E. Wyatt, The Journal of Chemical Physics 109, 10732 (1998), http://link.aip.org/link/?JCP/109/10732/1
- [28] M. Wilkinson and E. J. Austin, Phys. Rev. A 47, 2601 (Apr 1993)
- [29] E. S. Swanson, Phys. Rev. E 83, 040901 (Apr 2011), http://link.aps.org/doi/10.1103/PhysRevE.83.040901